Journal of Alloys and Compounds 731 (2018) 1119–1124

Contents lists available at ScienceDirect

Journal of Alloys and Compounds

journal homepage: http://www.elsevier.com/locate/jalcom

Role of crystallinity on the optical properties of $Na_2V_6O_{16}\cdot 3H_2O$ nanowires

W. Avansi [a, *], L.J.Q. Maia [b], H.A.J.L. Mourão [c], C. Ribeiro [d]

[a] Departamento de Física, Universidade Federal de São Carlos, São Carlos, SP, Brazil
[b] Grupo Física de Materiais, Instituto de Física, Universidade Federal de Goiás, Goiânia, GO, Brazil
[c] Instituto de Ciência e Tecnologia, Universidade Federal dos Vales do Jequitinhonha e Mucuri, Diamantina, MG, Brazil
[d] Embrapa Instrumentação, São Carlos, SP, Brazil

ARTICLE INFO

Article history:
Received 28 April 2017
Received in revised form
2 October 2017
Accepted 16 October 2017
Available online 18 October 2017

Keywords:
$Na_2V_6O_{16}\cdot 3H_2O$
1D-nanostructures
XANES spectroscopy
Photoluminescence spectroscopy

ABSTRACT

It is known that optical properties depend on crystalline structures, feature that can significantly affect materials such as vanadates, since their lamellar structures tend to be irregular. Synthetic methods, such as hydrothermal annealing, may enhance the understanding of the dependence, once fine crystallization control is possible. Consequently, a monoclinic phase of $Na_2V_6O_{16}\cdot 3H_2O$ 1D-nanostructures as nanowires has been obtained by decomposition of vanadium peroxide in hydrothermal conditions. X-ray diffraction (XRD), X-ray absorption spectroscopy (XAS) and high-resolution transmission electron microscopy (HRTEM) were employed to characterize the structure, local-order structure and morphology of the as-obtained samples. The optical and electronic properties of the samples were studied by photoluminescence (PL), UV–Visible diffuse reflectance (DRS) and electron paramagnetic resonance (EPR) spectroscopies. The nanostructures present a single crystalline nature and emit intense light at room temperature from 2.4 eV to 3.2 eV, i.e., from 520 nm to 390 nm, which is related to the crystalline nature of the samples. As the synthesis temperature increased, structural defects (V^{4+} centers) were reduced, and monocrystalline materials with improved PL from ultraviolet to green light emission could be obtained.

1. Introduction

One-dimensional nanostructured compounds of alkali-metal vanadium oxide have attracted the interest of many researchers due to their several range of applications [1–11]. More specifically, due to their structural and morphologic characteristics, the $Na_2V_6O_{16}\cdot nH_2O$ nanostructures can be potentially applied as anode materials [7], sensors [5], photocatalysts [8], among others [9–11], once they have a typical layered structure that permits hydrated sodium to be located at the interstices between V_3O_8 layers, which can then be called interstitial hydrated sodium (Na^+) [7,8]. For example, Zhang et al. [5] reported that gas sensing properties to alcohols and acetones present a better sensitivity when compared to V_2O_5 compounds. Feng et al. [8] showed that $Na_2V_6O_{16}\cdot 3H_2O$ nanoribbons present a promising photocatalytic activity for renewable hydrocarbon fuel (CH_4) in the presence of water vapor under visible-light irradiation.

Due to their interesting properties, these compounds have been obtained by several methods [1,2,4,9–18]. Nevertheless, our group previously reported a promising procedure to obtain $Na_2V_6O_{16}\cdot 3H_2O$ nanowires using an environmentally-friendly, one-step low temperature hydrothermal route [18]. This procedure has been considered very attractive due to its relative simplicity and the absence of organic or inorganic additives acting as templates and/or catalysts to the reaction system, enabling it to be free from undesired impurities. However, one aspect often neglected in this synthetic method is the habilitation of crystallinity control, which is a key parameter for many properties – specifically for optical properties, this parameter is very influent, although it has not been fully studied for sodium vanadates, leading to a lack of information about this subject.

Therefore, in this present study we report a correlation between structural and optical properties for the as-obtained $Na_2V_6O_{16}\cdot 3H_2O$ 1D nanostructures. The morphology and structure of the samples were examined by X-ray diffraction (XRD), high-resolution transmission electron microscopy (HRTEM), X-ray

* Corresponding author.
E-mail address: w_avansi@pq.cnpq.br (W. Avansi).

https://doi.org/10.1016/j.jallcom.2017.10.121
0925-8388/

absorption near-edge spectroscopy (XANES), and electron paramagnetic resonance (EPR) spectroscopy. The optical properties of the samples were also studied by UV–Visible diffuse reflectance (DRS) and photoluminescence (PL) spectroscopies.

2. Materials and methods

The samples were prepared by hydrothermal conditions at different treatment temperatures previously described in detail, see Ref. [18]. As reported earlier, the samples obtained by hydrothermal treatment at 200 °C exhibit similar structures to those treated at 140 °C, both during 24hrs [18]. In this sense, only the results relative to the sample treated at 140 °C (called SAM01) and to the one at 200 °C (called SAM02), both under extreme conditions, were discussed.

The crystalline structure was determined by X-ray diffraction (XRD) through a Shimadzu XRD 6100 diffractometer with Cu $K\alpha$ radiation in a continuous scan mode (2°/min with a step of 0.02°).

UV–visible diffuse reflectance spectra (DRS) were acquired employing a Shimadzu UV-2600 UV-VIS spectrophotometer in the 200–800 nm range, recalculated using the Tauc method and then normalized.[35] The band-gap of each sample was calculated by plotting the absorption coefficient, $(\alpha h\nu)^2$, against the photon energy, $h\nu$, according to the following equation: $\alpha h\nu = A(h\nu - E_g)^{1/2}$, where E_g describes the band gap for direct transitions and A is a constant.[35] The band gap energy of the studied samples could be thus obtained from the plots of $[F(R_\infty)h\nu]^2$ versus photon energy ($h\nu$), as shown in Fig. 2, where $R_\infty = R_{sample}/R_{reference}$, and $F(R_\infty) = (1-R_\infty)^2/(2R_\infty)$ [19].

Photoluminescence spectroscopy (PL) properties of the as-obtained samples were investigated by emission spectra obtained in a Fluorolog FL-322 Horiba/Jobin-Yvon spectrofluorimeter, with a 450 W xenon lamp for steady-state luminescence spectra, and a Hamamatsu photomultiplier. The emission was corrected using the spectral response of both the monochromators and the detector, which configures a typical correction spectrum provided by the manufacturer.

The XANES (X-ray absorption near-edge structure) spectrum was measured at the V K-edge using the D08B-XAFS2 beam line at the Brazilian Synchrotron Light Laboratory (LNLS). The Vanadium K-edge XANES spectra were collected in transmission mode at room temperature using a Si (111) channel-cut monochromator from 40 eV below and 80 eV above the edge with an energy step of 0.3eV near the edge region. XANES spectra of the samples deposited on polymeric membranes were collected with the sample placed at 90° relative to the X-ray beam. To provide good energy reproducibility during the XANES data collection, the energy calibration of the monochromator was checked using a V metal foil.

EPR measurements were performed in an EMX Bruker spectrometer working at 9.4 GHz (X-band), with standard Bruker rectangular cavities operating with a microwave power of 1 mW and 16 scans were collected from samples with the same mass for comparison. Magnetic external field could vary from 3400 to 3700 Gauss. Resonance field, intensity and peak-to-peak line width, ΔB_0, were determined from the EPR spectra, and the g-factor was calculated by the resonance condition equation: $g = h\nu/\mu_B B_0$, where h is the Planck constant, ν is the microwave frequency, μ_B is the Bohr magneton, and B_0 is the resonance magnetic field [20].

The samples were also studied by transmission electron microscopy (TEM), using a FEI-Tecnai operating at 200 KeV.

3. Results and discussions

In a previous work [18], we reported that the samples obtained at different temperature treatments reveal similar structural results, observed by XRD patterns and shown in Fig. 1. The XRD patterns for these samples, SAM01 and SAM02, confirm the formation of the $Na_2V_6O_{16}\cdot 3H_2O$ monoclinic phase, with lattice parameters: $a = 12.17$ Å, $b = 3.602$ Å and $c = 7.78$ Å, with $\beta = 95.03°$ (JCPDS file n° 16-0601). Nevertheless, from Fig. 1 we can observe small peaks at around 20.9 and 27.4^0 (both peaks identified by *) not identified before, related to a small quantity of impurity phases. Additionally, we can note another small peak around 29.7° (denoted as #), related to the dehydrated $Na_2V_6O_{16z}$ phase (JCPDS file no. 22-1412). The water content and thermal stability of the samples were checked by thermogravimetric analysis (TGA), not shown here, and they do not present any significant changes for both samples, once the water content was considered similar to the one previously observed by our group and found in literature [17,18].

The DRS spectra of the as-obtained samples are shown in Fig. 2, which illustrates the absorption spectra obtained from the Kubelka-Munk equation in order to calculate the band gap of the samples, Fig. 2b [19]. According to Fig. 2, no significant changes on the bandgap values could be observed. Such values were estimated from the intercept of the tangents to the plots equal to 1.94 eV and 1.93 eV for SAM01 and SAM02, respectively. These results are quite similar to the ones reported by Feng et al. [8], clearly demonstrating that electronic structures of the samples were not significantly changed by the temperature treatment of hydrothermal synthesis.

Fig. 3a and b presents the PL spectra of SAM01 and SAM02, respectively, under several excitation wavelengths (λ_{exc}). It is interesting to note that the PL spectra of SAM01 present significantly smaller intensity concerning the emission from 2.4 to 3.2eV compared to those of SAM02. Indeed, despite several λ_{exc}, from Fig. 3b it can be observed that the SAM02 samples present a PL with high intensity and broad emission from 2.4 eV to 3.2 eV at room temperature, from 520 nm to 390 nm. The observed PL emissions in this region cannot be related to the band edge transition, since according to the band gap obtained earlier, see Fig. 2, the as-synthesized nanostructures have a band gap around 1.9 eV, which appears to be a significant band emission for SAM01. It is worth noting that the maximum emissions are observed under the excitation at 390 nm, refer to Fig. 3c, where the emission energies remains constant, even with different λ_{exc}, refer to Fig. 3b. Recently, some papers have reported the PL properties of vanadates compounds [21–25], commonly attributing the PL intensity of vanadate compounds to defects in crystal structure, such as O vacancy, V vacancy and/or O interstitial [21,22,26,27]. On the other hand, our

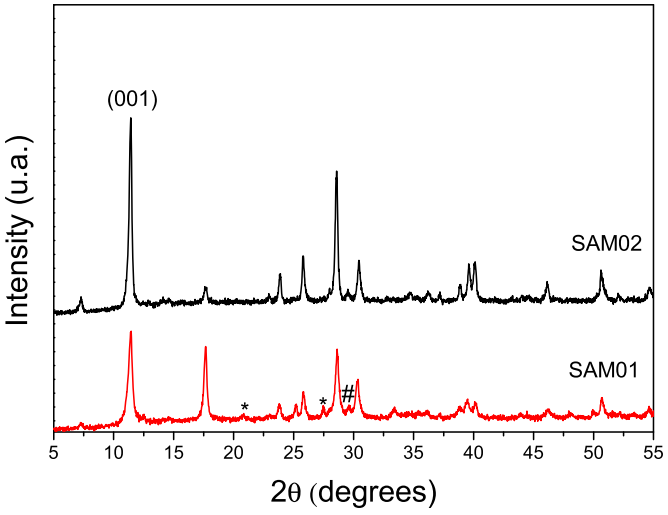

Fig. 1. XRD patterns of the as-obtained samples SAM01 and SAM02.

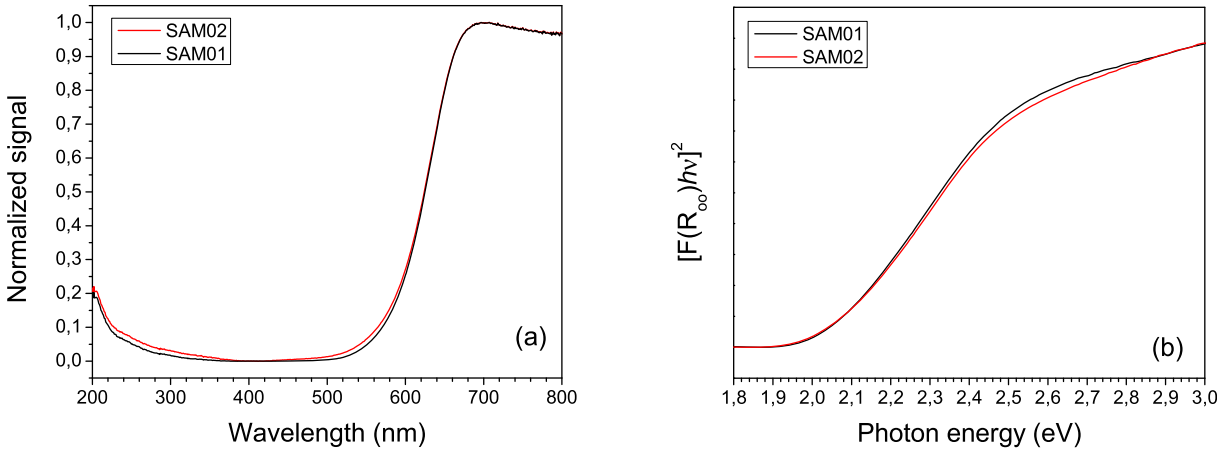

Fig. 2. (a) UV–visible diffuse reflectance spectra (DRS) normalized and (b) absorption spectra obtained from Kubelka-Munk equation [19] for the as-synthesized samples.

group previously showed that the emission of visible light at room temperature regarding V_2O_5 nanostructures obtained by hydrothermal method could be related to the local order of V atoms of the studied samples [28].

Over the last years, our group has been applying the XAS spectroscopy in order to check the local order of the studied samples obtained in different synthetic conditions, especially in XANES regions [18,28–32]. Fig. 4 shows the normalized V-K XANES spectra of the synthesized samples (SAM01 and SAM02) compared to the V_2O_5 orthorhombic crystalline phase employed as a reference compound. From Fig. 4, it is clear that the main difference among the XANES spectra is related to variations in oscillations after the edge. The pre-edge peak is attributed for several papers to the transition from V 1s to V 3d states forbidden by the dipole selection rules in centrosymmetric systems, yet allowed in non-centrosymmetric systems via hybridization between V 3d and O 2p states [29,33–36]. As a matter of fact, several papers associated the intensity of the pre-edge peak with a strong dependence on the local structure around vanadium atoms, indicated by the degree of distortion of the first shell oxygen atoms [29,35–37]. Although the V_2O_5 orthorhombic phase is composed of VO_5 octahedral units [28,29,36] while $Na_2V_6O_{16}\cdot 3H_2O$ is composed of VO_6 octahedral units [38], the analysis of the pre-edge peak of these two samples shows that the local structure around vanadium atoms are quite similar, see Fig. 4, as reported previously by our group [18]. Fig. 4 also reveals that the energy of the pre-edge peak region and their respective first derivative in sample SAM02 are similar to the V_2O_5 orthorhombic phase. As the pre-edge and the main edge energy are sensitive to variations in the oxidation state of vanadium atoms [28,31], the oxidation state of vanadium atoms in $Na_2V_6O_{16}\cdot 3H_2O$ nanowires is comparable to the reference compound, i.e., V^{5+}, in good agreement with our previous work. Nevertheless, Zhou et al. who observed the presence of a mixed valence (V^{4+} and V^{5+}) in a $Na_2V_6O_{16}\cdot 3H_2O$ nanostructured compound [17]. In the post-edge region, the XANES spectra of SAM01 and SAM02 reveals some differences related to the spectrum of the reference compound (V_2O_5 orthorhombic phase) and compared to each other. The difference with reference compound is expected due to their distinct crystalline phase, nevertheless, the post-edge region of the XANES spectra of SAM01 and SAM02 were slightly distinct. The SAM01 spectra had a smooth aspect compared to SAM02, mainly from around 4490 to 5520eV, which can be related to a greater disorder around the vanadium atoms [29,33–36].

Besides XANES spectroscopy, in order to further investigate the occurrence of oxygen vacancies or other defects and explain the PL origin emissions EPR spectroscopy was applied, (Fig. 5), since the high sensitivity of this technique permits the determination of low concentration of paramagnetic centers [39,40]. Resonance field, intensity, peak-to-peak line width, ΔB_0, all determined from the EPR spectra, as well as calculated g-factor, were listed in Table 1.

From Table 1, it is to possible observe that the paramagnetic signal of $g = 1.89$ decreases in its intensity as the synthesis temperature increases (from 140 °C to 200 °C). Some papers studied vanadium compounds though EPR technique [20,39–42]. Yablokov and co-workers [41] observed an EPR signal for g around 1.98, which was explained by intramolecular electron transfers into $V^{4+}{}_4V^{5+}{}_2O_7(OCH_3)_{12}$ compounds, i.e., the transfers of the excess electron between $V^{4+} - V^{5+}$ states. Additionally, J. Deisenhofer and collaborators [42] observed a g-factor around 1.87 at room temperature for Sr_2VO_4 compounds with orthorhombic symmetry due to two crystallographically inequivalent vanadium sites. D. Gourier et al. [20] studied the lithium intercalation in V_2O_5 cathodes using EPR and observed $g_{\|}$ and $g_{\perp}$ factors of 1.923 and 1.982, respectively, which were attributed to an electron-hole defect in $Li_xV_2O_5$, originated from a local charge compensation of vanadyl vacancies. In fact, the formation of O^- hole defects in $Li_xV_2O_5$ only constitutes a local charge compensation for vanadyl vacancies. Molochnikov and co-workers [43] observed a g-factor of 1.897 for $Ti_{0.83}V_{0.17}O_{2+\delta}\cdot nH_2O$ xerogels related to V^{4+} paramagnetic centers. Then, we can conclude that g-factor of 1.89 in the $Na_2V_6O_{16}\cdot 3H_2O$ nanocrystals observed in this work could be related to V^{4+} paramagnetic centers not well discriminated by XANES spectra probably due to their low concentration in comparison with V^{5+} ions. Since the paramagnetic signal of $g = 1.89$ decreases their intensity as the synthesis temperature increases (from 140 °C to 200 °C), it is expected that the V^{4+} paramagnetic centers also decrease. Even though PL properties of vanadates compounds are commonly attributed to defects in crystal structure [21,22,26,27], our results indicated that the higher presence of paramagnetic centers leads to a decrease in PL intensity, where the defects present in the structure act as PL quencher [44]. Indeed, the XANES and EPR results reveal that the sample obtained at higher temperature (SAM02) possesses fewer defects in crystal structure.

The HRTEM image of SAM02, see Fig. 6(a) and (b), reveals the monocrystalline nature of these samples, where the interplanar distance calculated is about 1.23 nm, consistent with (100) plane in the $Na_2V_6O_{16}\cdot 3H_2O$ monoclinic phase, as observed in XRD patterns. This fact differs from what was observed earlier for the sample obtained at 140 °C (SAM01), since the HRTEM results showed a polycrystalline nature for such samples [18].

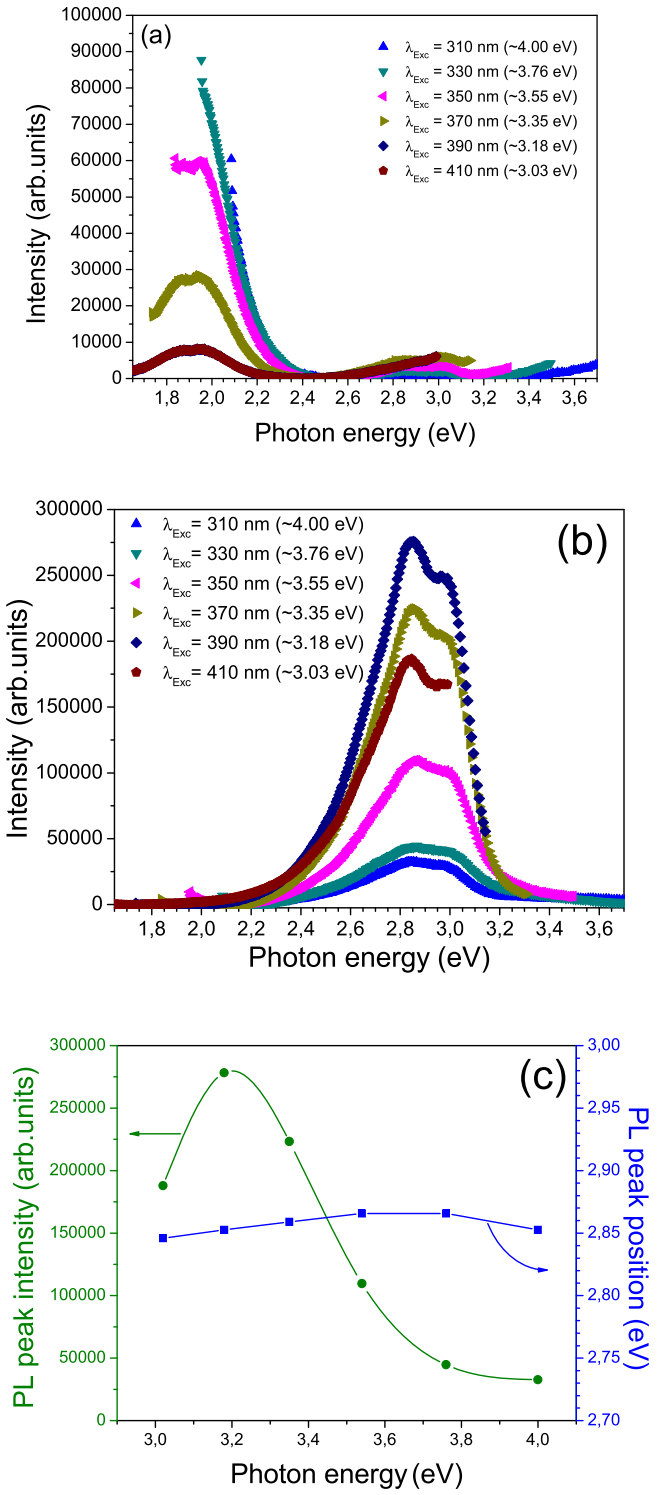

Fig. 3. (a) and (b) The room-temperature PL spectra for the SAM01 and SAM02, respectively; and (c) peak intensity and position of the maximum PL spectra versus energy of excitation (λ_{exc}) of the as-synthesized SAM02.

Despite the fact that $Na_2V_6O_{16}\cdot 3H_2O$ obtained under different hydrothermal temperatures presented expected differences in size, the PL properties of these samples also appear to be related to the surface of such structures. The high PL intensity of the samples obtained at 200 °C (SAM02) could also be related to their monocrystalline nature, since, as reported, the samples obtained at

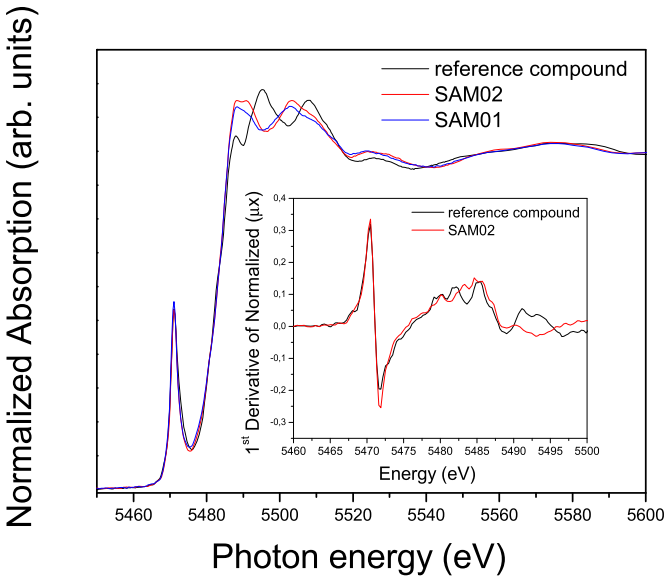

Fig. 4. Normalized Vanadium K-edge XANES spectra of reference compound (V_2O_5 orthorhombic phase) and the SAM01 and SAM02. Inset: An expanded view of the first derivative of the pre-edge region for the sample SAM02 and reference compound.

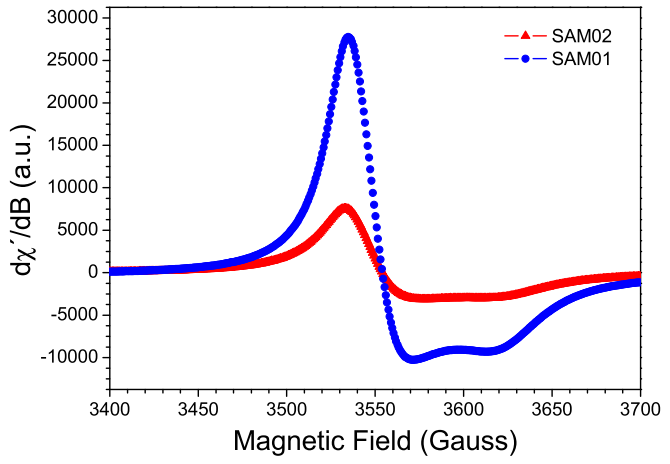

Fig. 5. EPR spectra of the SAM01 and SAM02 samples, taken at room temperature.

140 °C (SAM01) showed a polycrystalline nature. In this sense, the higher presence of structural defects observed in SAM01 can become centers to capture photo-induced electrons so that the recombination of photo-induced electrons and holes can be inhibited [45].

4. Conclusions

In summary, this work aimed to study the structural, spectroscopic and electronic properties of the $Na_2V_6O_{16}\cdot 3H_2O$ monoclinic phase composed of nanowires and synthesized by a simple, environmentally-friendly hydrothermal method. The formed $Na_2V_6O_{16}\cdot 3H_2O$ at the highest temperature studied could emit intense light at room temperature from 2.4 eV to 3.2 eV, i.e., from 520 nm to 390 nm. According to the results, high PL intensities in the sample synthesized at the highest temperature are related to the monocrystalline nature and the low concentration of defects, such as V^{4+} centers. This study might provide a simple route in order to obtain nanostructures with required properties just by

Table 1
Values of resonance field, intensity, peak-to-peak line width ΔB_0, and *g*-factor for SAM01 and SAM02 samples.

Sample	Resonance field (Gauss)	Intensity (arb.units)	peak-to-peak line width ΔB_0 (Gauss)	*g*-factor
SAM01	3554.1	38025	36.4	1.89
SAM02	3554.2	10707	45.3	1.89

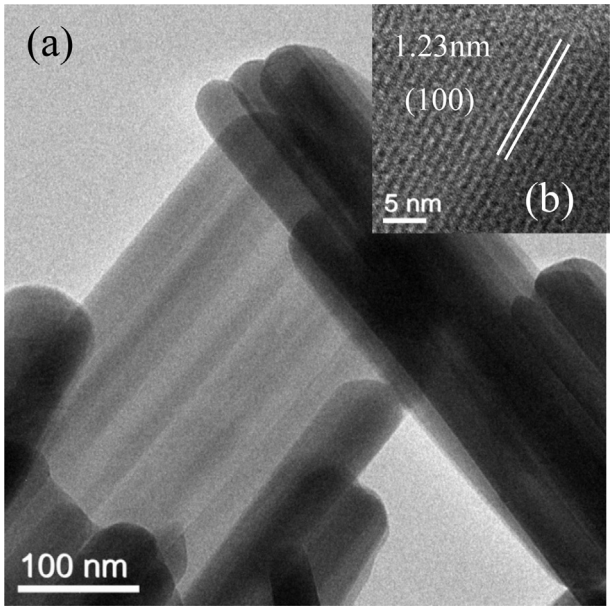

Fig. 6. (a) TEM and (b) HRTEM images of the sample obtained at 200 °C for 24 h.

selecting the hydrothermal synthesis conditions and modulating the photoluminescence emissions.

Acknowledgements

The authors gratefully acknowledge the financial support of the Brazilian research funding agencies: FAPESP (2013/17639-4), FAPEG (201200555800717 and 201510267000184), CAPES (88881.121134/2016-01) and CNPq (310863/2014-7, 454438/2014-1, 407966/2013-7 and 460089/2014-5). XANES measurements facilities were provided by LNLS-Campinas, SP, Brazil (research proposal number 10972). HRTEM/TEM facilities were provided by LCE (Department of Materials Science, UFSCar, São Carlos, SP, Brazil).

References

[1] C.V.S. Reddy, I.H. Yeo, S.I. Mho, Synthesis of sodium vanadate nanosized materials for electrochemical applications, J. Phys. Chem. Solids 69 (2008) 1261–1264.
[2] S.H. Lim, J.Y. Lin, Y.W. Zhu, C.H. Sow, W. Ji, Synthesis, characterizations, and field emission studies of crystalline $Na_2V_6O_{16}$ nanobelt paper, J. Appl. Phys. 100 (2006), 0161105.
[3] S. Jouanneau, A. Verbaere, D. Guyomard, On a new calcium vanadate: synthesis, structure and Li insertion behavior, J. Solid State Chem. 172 (2003) 116–122.
[4] S. Jouanneau, A.L. La Salle, A. Verbaere, D. Guyomard, M. Deschamps, S. Lascaud, New alkaline earth substituted lithium trivanadates: synthesis, characterization and lithium insertion behavior, J. Mater. Chem. 13 (2003) 1827–1834.
[5] Z. Zhang, Y.V. Kaneti, X. Jiang, A. Yu, Hydrothermal synthesis of sodium vanadium oxide nanorods for gas sensing application, Sensors Actuators B-Chem. 202 (2014) 803–809.
[6] Q. Tan, Q. Zhu, A. Pan, Y. Wang, Y. Tang, X. Tan, S. Liang, G. Cao, Template-free synthesis of beta-$Na_{0.33}V_2O_5$ microspheres as cathode materials for lithium-ion batteries, Crystengcomm 17 (2015) 4774–4780.
[7] C. Deng, S. Zhang, Z. Dong, Y. Shang, 1D nanostructured sodium vanadium oxide as a novel anode material for aqueous sodium ion batteries, Nano Energy 4 (2014) 49–55.
[8] S. Feng, X. Chen, Y. Zhou, W. Tu, P. Li, H. Li, Z. Zou, $Na_2V_6O_{16}$ center dot $xH_{(2)}O$ nanoribbons: large-scale synthesis and visible-light photocatalytic activity of CO2 into solar fuels, Nanoscale 6 (2014) 1896–1900.
[9] W.D. Zhang, G.B. Xu, L.W. Yang, J.W. Ding, Ultra-long $Na_2V_6O_{16}$ center dot xH(2)O nanowires: large-scale synthesis and application in binder-free flexible cathodes for lithium ion batteries, Rsc Adv. 6 (2016) 5161–5168.
[10] Y.S. Cai, J. Zhou, G.Z. Fang, G.M. Cai, A.Q. Pan, S.Q. Liang, Na0.282V2O5: a high-performance cathode material for rechargeable lithium batteries and sodium batteries, J. Power Sources 328 (2016) 241–249.
[11] S. Hartung, N. Bucher, J.B. Franklin, A.M. Wise, L.Y. Lim, H.Y. Chen, J.N. Weker, M.E. Michel-Beyerle, M.F. Toney, M. Srinivasan, Mechanism of Na+ insertion in alkali vanadates and its influence on battery performance, Adv. Energy Mater. 6 (2016) 1502336.
[12] S. Iwanaga, M. Marciniak, R.B. Darling, F.S. Ohuchi, Thermopower and electrical conductivity of sodium-doped V_2O_5 thin films, J. Appl. Phys. 101 (2007) 123709.
[13] H.M. Liu, Y.G. Wang, L. Li, K.X. Wang, E. Hosono, H.S. Zhou, Facile synthesis of NaV_6O_{15} nanorods and its electrochemical behavior as cathode material in rechargeable lithium batteries, J. Mater. Chem. 19 (2009) 7885–7891.
[14] J.G. Yu, J.C. Yu, W.K. Ho, L. Wu, X.C. Wang, A simple and general method for the synthesis of multicomponent $Na_2V_6O_{16}$ center dot 3H(2)O single-crystal nanobelts, J. Am. Chem. Soc. 126 (2004) 3422–3423.
[15] O. Durupthy, N. Steunou, T. Coradin, J. Maquet, C. Bonhomme, J. Livage, Influence of pH and ionic strength on vanadium(V) oxides formation. From V_2O_5 center dot $nH_{(2)}O$ gels to crystalline NaV_3O_8 center dot $1.5H_{(2)}O$, J. Mater. Chem. 15 (2005) 1090–1098.
[16] L. Bouhedja, N. Steunou, J. Maquet, J. Livage, Synthesis of polyoxovanadates from aqueous solutions, J. Solid State Chem. 162 (2001) 315–321.
[17] G.T. Zhou, X.C. Wang, J.C. Yu, Selected-control synthesis of NaV_6O_{15} and $Na_2V_6O_{16}$ center dot $3H_{(2)}O$ single-crystalline nanowires, Cryst. Growth & Des. 5 (2005) 969–974.
[18] W. Avansi Jr., C. Ribeiro, E.R. Leite, V.R. Mastelaro, An efficient synthesis route of Na2V6O16 center dot nH(2)O nanowires in hydrothermal conditions, Mater. Chem. Phys. 127 (2011) 56–61.
[19] K. Suzuki, K. Kijima, Optical band gap of barium titanate nanoparticles prepared by RF-plasma chemical vapor deposition, Jpn. J. Appl. Phys. Part 1-Regular Pap. Brief Commun. Rev. Pap. 44 (2005) 2081–2082.
[20] D. Gourier, A. Tranchant, N. Baffier, R. Messina, EPR study of electrochemical lithium intercalation in V_2O_5 cathodes, Electrochim. Acta 37 (1992) 2755–2764.
[21] B. Yan, L. Liao, Y.M. You, X.J. Xu, Z. Zheng, Z.X. Shen, J. Ma, L.M. Tong, T. Yu, Single-crystalline V_2O_5 ultralong nanoribbon waveguides, Adv. Mater. 21 (2009) 2436–2440.
[22] Y.Q. Wang, Z.C. Li, X. Sheng, Z.J. Zhang, Synthesis and optical properties of V_2O_5 nanorods, J. Chem. Phys. 126 (2007) 164701.
[23] V.G. Pol, S.V. Pol, J.M. Calderon-Moreno, A. Gedanken, Core-shell vanadium oxide-carbon nanoparticles: synthesis, characterization, and luminescence properties, J. Phys. Chem. C 113 (2009) 10500–10504.
[24] K. Teramura, T. Hosokawa, T. Ohuchi, T. Shishido, T. Tanaka, Photoactivation mechanism of orthovanadate-like $(V = O)O^{-3}$ species, Chem. Phys. Lett. 460 (2008) 478–481.
[25] T. Nakajima, M. Isobe, T. Tsuchiya, Y. Ueda, T. Manabe, Photoluminescence property of vanadates $M_2V_2O_7$ (M: Ba, Sr and Ca), Opt. Mater. 32 (2010) 1618–1621.
[26] C. Diaz-Guerra, J. Piqueras, Thermal deposition growth and luminescence properties of single-crystalline V_2O_5 elongated nanostructures, Cryst. Growth & Des. 8 (2008) 1031–1034.
[27] Y. Hu, Z.C. Li, Z.J. Zhang, D.Q. Meng, Effect of magnetic field on the visible light emission of V_2O_5 nanorods, Appl. Phys. Lett. 94 (2009) 103107.
[28] W. Avansi, L.J.Q. Maia, C. Ribeiro, E.R. Leite, V.R. Mastelaro, Local structure study of vanadium pentoxide 1D-nanostructures, J. Nanoparticle Res. 13 (2011) 4937–4946.
[29] W. Avansi, C. Ribeiro, E.R. Leite, V.R. Mastelaro, Vanadium pentoxide nanostructures: an effective control of morphology and crystal structure in hydrothermal conditions, Cryst. Growth & Des. 9 (2009) 3626–3631.
[30] L.F. da Silva, W. Avansi Jr., J. Andres, C. Ribeiro, M.L. Moreira, E. Longo, V.R. Mastelaro, Long-range and short-range structures of cube-like shape $SrTiO_3$ powders: microwave-assisted hydrothermal synthesis and photocatalytic activity, Phys. Chem. Chem. Phys. 15 (2013) 12386–12393.
[31] L.F. da Silva, W. Avansi, M.L. Moreira, A. Mesquita, L.J.Q. Maia, J. Andres, E. Longo, V.R. Mastelaro, Relationship between crystal shape, photoluminescence, and local structure in $SrTiO_3$ synthesized by microwave-assisted hydrothermal method, J. Nanomater. (2012).
[32] M.L. Moreira, V.M. Longo, W. Avansi Jr., M.M. Ferrer, J. Andres, V.R. Mastelaro, J.A. Varela, E. Longo, Quantum mechanics insight into the microwave nucleation of $SrTiO_3$ nanospheres, J. Phys. Chem. C 116 (2012) 24792–24808.
[33] A.N. Mansour, P.H. Smith, M. Balasubramanian, J. McBreen, In situ x-ray absorption study of cycled ambigel V_2O_5 center dot n H_2O(n approximate to 0.5) composite cathodes, J. Electrochem. Soc. 152 (2005) A1312–A1319.
[34] A.N. Mansour, P.H. Smith, W.M. Baker, M. Balasubramanian, J. McBreen, Comparative in situ X-ray absorption spectroscopy study of nanophase V_2O_5 aerogel and ambigel cathodes (vol 150, pg A403, 2003), J. Electrochem. Soc.

150 (2003). L13–L13.
[35] A.N. Mansour, S. Dallek, P.H. Smith, W.M. Baker, Thermogravimetry and X-ray absorption spectroscopy study of heated V_2O_5 center dot $nH_{(2)}O$ aerogels and ambigels, J. Electrochem. Soc. 149 (2002) A1589–A1597.
[36] S. Stizza, G. Mancini, M. Benfatto, C.R. Natoli, J. Garcia, A. Bianconi, Structure of oriednted V_2O_5 gel studied by polarized x-ray-absorption spectrocopy at the vanadium K edge, Phys. Rev. B 40 (1989) 12229–12236.
[37] M. Giorgetti, S. Passerini, W.H. Smyrl, M. Berrettoni, Evidence of bilayer structure in V_2O_5 xerogel, Inorg. Chem. 39 (2000) 1514–1517.
[38] A.D. Wadsley, The crystal structure of $Na_{2-x}V_6O_{15}$, Acta Crystallogr. 8 (1955) 695–701.
[39] E. Giamello, Reactive intermediates formed upon electron transfer from the surface of oxide catalysts to adsorbed molecules, Catal. Today 41 (1998) 239–249.
[40] J. Matta, D. Courcot, E. Abi-Aad, A. Aboukais, Identification of vanadium oxide species and trapped single electrons in interaction with the $CeVO_4$ phase in vanadium-cerium oxide systems. V-51 MAS NMR, EPR, Raman, and thermal analysis studies, Chem. Mater. 14 (2002) 4118–4125.
[41] Y.V. Yablokov, M.A. Augustyniak-Jablokow, S. Borshch, C. Daniel, H. Hartl, Intramolecular and lattice dynamics in $(V_{6-n}V_nO_7)$-V-IV-O-V$(OCH_3)_{(12)}$ crystal, Acta Phys. Pol. A 108 (2005) 271–281.
[42] J. Deisenhofer, S. Schaile, J. Teyssier, Z. Wang, M. Hemmida, H.A.K. von Nidda, R.M. Eremina, M.V. Eremin, R. Viennois, E. Giannini, D. van der Marel, A. Loidl, Electron spin resonance and exchange paths in the orthorhombic dimer system Sr_2VO_4, Phys. Rev. B 86 (2012).
[43] L.S. Molochnikov, G.S. Zakharova, E.V. Mel'gunova, V.L. Volkov, Coordination of V^{4+} in vanadium titanium oxide xerogels, Inorg. Mater. 41 (2005) 1189–1193.
[44] G. Liu, J.E. Greedan, Synthesis, crystal-structures, and magnetic-properties of layered vanadium-oxides - $a_{(2)}V_{(4)}O_{(9)}$ (A=RB, CS), J. Solid State Chem. 115 (1995) 174–186.
[45] L.Q. Jing, X.J. Sun, B.F. Xin, B.Q. Wang, W.M. Cai, H.G. Fu, The preparation and characterization of La doped TiO_2 nanoparticles and their photocatalytic activity, J. Solid State Chem. 177 (2004) 3375–3382.